

ARTICLE OPEN



Characterizing the tumor suppressor activity of FLCN in Birt-Hogg-Dubé syndrome cell models through transcriptomic and proteomic analysis

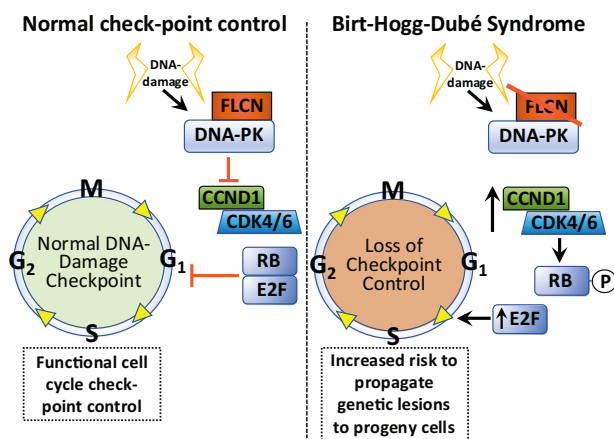
Rachel-Ann Jones ¹, Elaine A. Dunlop ¹, Jesse D. Champion¹, Peter F. Doubleday ^{1,2}, Tijs Claessens¹, Zahra Jalali³, Sara Seifan ¹, Iain A. Perry ¹, Peter Giles¹, Oliver Harrison¹, Barry J. Coull⁴, Arjan C. Houweling⁵, Arnim Pause³, Bryan A. Ballif² and Andrew R. Tee ^{1✉}

© The Author(s) 2025

Birt-Hogg-Dubé syndrome (BHD) patients are uniquely susceptible to all renal tumor subtypes. However, the underlying mechanism of carcinogenesis is unclear. To study cancer development in BHD, we used human proximal kidney (HK2) cells and found that long-term folliculin (*FLCN*) knockdown was required to increase the tumorigenic potential of these cells, as evidenced by the formation of larger spheroids under nonadherent conditions. Transcriptomic and proteomic analyses revealed links between the *FLCN*, cell cycle control and DNA damage response (DDR) machinery. In addition, HK2 cells lacking *FLCN* had an altered transcriptome profile and enriched cell cycle control genes. G₁/S cell cycle checkpoint signaling was compromised by increased protein levels of cyclin D1 (CCND1) and hyperphosphorylation of retinoblastoma 1 (RB1). A *FLCN* interactome screen revealed that *FLCN* binds to DNA-dependent protein kinase (DNA-PK). This novel interaction was reversed in an irradiation-responsive manner. Knockdown of *FLCN* in HK2 cells caused a marked increase in γH2AX and RB1 phosphorylation. The levels of both CCND1 and phosphorylated RB1 remained high during DNA damage, which was associated with defective cell cycle control caused by *FLCN* knockdown. Furthermore, *Flcn*-knockdown *C. elegans* were defective in cell cycle arrest caused by DNA damage. This work revealed that long-term *FLCN* loss and associated cell cycle defects in BHD patients could contribute to their increased risk of cancer.

Oncogene; <https://doi.org/10.1038/s41388-025-03325-z>

Graphical Abstract



INTRODUCTION

Birt-Hogg-Dubé syndrome (BHD, OMIM # 135150) is an autosomal dominant condition clinically characterized by fibrofolliculomas,

pneumothorax associated with multiple lung cysts and early-onset multiple renal cell cancers (RCC) [1, 2]. BHD is caused by inactivating germline variants in the *FLCN* (folliculin) gene [2]. The lifetime risk of

¹Division of Cancer and Genetics, Cardiff University, Heath Park, Cardiff CF14 4XN, UK. ²Department of Biology, University of Vermont, Marsh Life Science 311, 109 Carrigan Drive, Burlington, VT, USA. ³Department of Biochemistry and Goodman Cancer Institute, McGill University, Montréal, QC, Canada. ⁴Lancaster Medical School, Lancaster University, Lancaster LA1 4AT, UK. ⁵Department of Human Genetics, Amsterdam UMC, Vrije Universiteit Amsterdam, Amsterdam, The Netherlands. ✉email: tea@cardiff.ac.uk

Received: 31 May 2024 Revised: 24 January 2025 Accepted: 21 February 2025

Published online: 25 March 2025

RCC in patients with BHD has been estimated to be approximately 15%. BHD patient renal tumors may present as a variety of histological subtypes, including mixed forms [3]. Most BHD-related renal cell cancers grow slowly, but metastatic disease may present as the first manifestation of the disease. Surveillance for early detection of renal lesions and surgical treatment of localized RCC are based on insight into the biological behavior of these tumors. Many BHD patients develop multiple bilateral renal tumors, and nephron-sparing surgery is therefore essential [2]. There is evidence of biallelic inactivation of *FLCN* in many BHD RCCs. Targeted treatments for such tumors are not currently available due to a lack of basic understanding of the key pathways involved in tumor growth.

Although major advances have been made, the underlying mechanism of how BHD tumors develop over time has not been determined. Current evidence indicates that the core function of *FLCN* is in lysosomal nutrient sensing and autophagy control through *FLCN*'s control of the Rag GTPases and thus mechanistic target of rapamycin (mTOR) phosphorylation of TFE3 and TFEB [4–7]. Further crosstalk with lysosomal pathways likely occurs via both AMPK- and ULK1-mediated phosphorylation of *FLCN* [8] and TFE3/TFEB phosphorylation via AMPK [9]. As a direct or indirect result of lysosomal dysfunction, loss of *FLCN* can cause abnormal ciliogenesis [10] and defects in metabolic homeostasis [11, 12], with the metabolic shift seen in BHD cells resulting from *FLCN* inactivation or dissociation from LDHA [13]. *FLCN* has also been linked to a variety of fundamental cellular processes, including cell adhesion through plakophilin-4 (PKP4) [14, 15], cell growth and division through rRNA synthesis [16], cyclin D1 (*CCND1*) and marked changes in gene expression [17]. RagC-independent functions of *FLCN* have also been revealed in recent research, where *FLCN* was found to be a Rab7A GTPase-activating protein involved in endocytic trafficking of epidermal growth factor receptor [18]. A related novel hereditary disorder was linked to *PR/SET domain 10* (*PRDM10*), which predisposes families to skin and mucosal lesions, lipomatosis and renal cell carcinomas [19, 20]. The *PRDM10* mutation that cosegregated with disease was found to be defective at binding to *FLCN* promoter regions and consequently caused a reduction in *FLCN* expression [19].

Although the involvement of *FLCN* in cell growth control is better understood, it is still not clear how dysregulation of this pathway following *FLCN* loss could predispose patients to multiple RCC subtypes with different mutational signatures [21]. Therefore, we wanted to further study the tumorigenic mechanisms underlying *FLCN* loss. To do this, we studied a human kidney proximal tubule (HK2) cell line, as proximal tubule cells in the kidney are considered to be the origin cell in BHD tumor formation [22–24]. We observed increased tumorigenic properties after long-term knockdown of *FLCN* in HK2 cells (after they had been cultured for one year), while short-term *FLCN* knockdown had little ability to transform these cells. We examined the transcriptome profiles of these cells to reveal the enrichment of genes linked to cell cycle control, a tumorigenic feature that became more prominent with long-term loss of *FLCN*. To better understand the function of *FLCN*, we then carried out proteomic analysis of *FLCN* interactors, which were also mapped to multiple cell cycle regulators and included components of the DNA damage machinery. Our findings suggest that alterations in cell cycle control upon *FLCN* loss enhance cancer progression in patients with BHD.

RESULTS

Long-term knockdown of *FLCN* increases tumorigenesis

To mimic long-term haploinsufficiency of *FLCN* in kidney cells from BHD patients, we continuously grew HK2 cells, a human proximal tubule cell line, with or without *FLCN* knockdown for one year in tissue culture to determine the long-term effects of *FLCN* knockdown. To compare short-term effects, cells were grown for

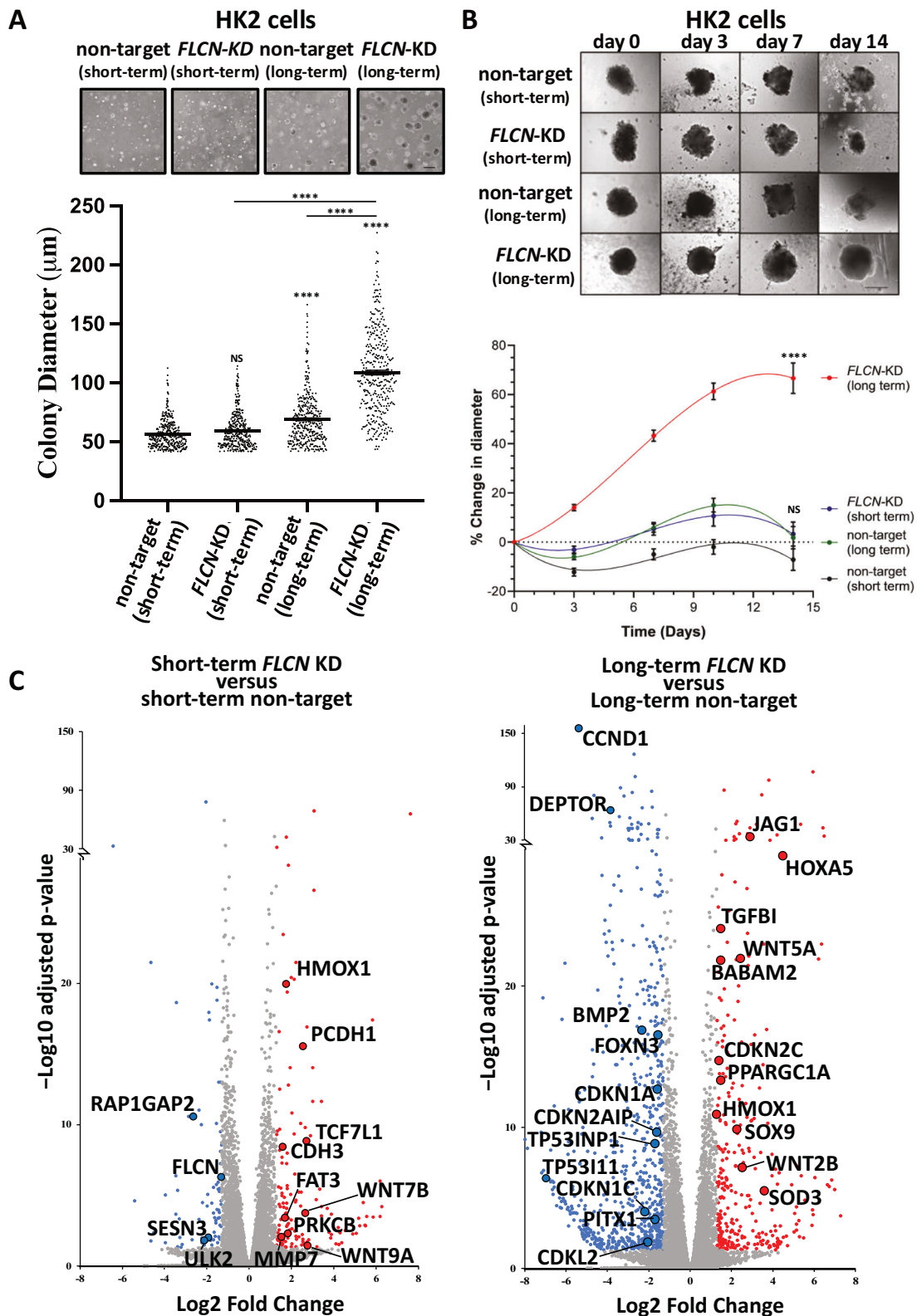
<2 months after *FLCN* knockdown. To investigate whether long-term *FLCN* deficiency increases tumorigenicity, we compared the growth of these *FLCN*-knockdown HK2 cells in soft agar (Fig. 1A). Short-term *FLCN* knockdown did not alter colony formation, while long-term *FLCN* knockdown led to markedly larger colonies, with a mean diameter >100 μm . Colony diameters within the long-term *FLCN* knockdown population were more divergent, indicating heterogeneity in colony formation.

To further assess anchorage-independent growth, these HK2 cells were grown as self-aggregated spheroids (Fig. 1B). We observed greater tumorigenicity after long-term *FLCN* knockdown than after short-term *FLCN* knockdown. We next analyzed the spheroid growth of additional nontarget and *FLCN* shRNA-knockdown clones (Supplementary Fig. 1), which supported our finding that long-term *FLCN* knockdown cells presented the greatest increase in spheroid diameter. These data revealed that long-term *FLCN* knockdown has a greater capacity to promote tumorigenicity than short-term *FLCN* knockdown.

FLCN knockdown dramatically altered the transcriptome profile over time, as indicated by gene enrichment of cell cycle genes

Changes in transcription between nontarget HK2 cells and HK2 cells with *FLCN* knockdown were investigated. A PCA and Euclidean cluster dendrogram plot of DESeq2-normalized samples showed that the experimental replicates clustered tightly into distinct groups. The most significant factor of interest (PC1) separated the long-term *FLCN* knockdown group from all the other groups (Supplementary Fig. 2A, B). While short-term *FLCN* knockdown altered the expression of 216 genes, this number of genes strikingly increased to 1063 after long-term *FLCN* knockdown (Fig. 1C; ≥ 2.5 -fold change up or down, $\text{padj} < 0.05$ with false rate discovery (FDR) correction applied). We also observed that ageing alone altered 250 gene transcripts by at least two-fold in the control cells, but 3.4 times more genes had altered gene expression when *FLCN* loss was combined with ageing. A WNT signaling signature was evident after both short- and long-term *FLCN* knockdown. The DEGs associated with long-term *FLCN* knockdown showed the greatest enrichment in 'Aberrant regulation of mitotic G₁/S transition in cancer due to RB1 defects', Reactome: R-HSA-9659787 (> 100-fold enrichment and 7.65E-04 FDR correction applied). Therefore, we investigated the involvement of RB1/E2F-regulated genes in S-phase entry. When comparing short-term *FLCN* knockdown to its wild-type control (Fig. 2A), *TGFA*, *CCND1*, *PPARGC1A* (also known as *PGC1a*) and *CDKN1C* were upregulated with *FLCN* knockdown. After long-term *FLCN* knockdown, many additional genes were differentially expressed. The three *HOX* genes exhibited the greatest increase in expression, while *TP53*, *BMP2*, *TGFA* and *CCND1* were downregulated (Fig. 2B). Changes in the expression of the E2F-regulated genes *CCND1*, *TP53*, *PPARGC1A*, *TGFA*, *c-Jun*, *RPA1* and *RBL1* [25] are shown in Fig. 2C, as are *p21* (*CDKN1A*) and *FOXN3*, which can arrest cells at the G₁ checkpoint [26, 27]. The mRNA expression levels of *CCND1*, *TP53*, *FOXN3*, *p21* (*CDKN1A*), *TGFA* and *CCNE1* were downregulated after long-term *FLCN* knockdown. In support of these observed alterations in cell cycle regulatory components, compared with wild-type cells, *FLCN* knockdown cells presented small but significant changes in 2N (G₀/G₁) and 4N (G₂/M) expression according to flow cytometry (Supplementary Fig. 2C).

To determine dysregulation at the pathway level, we assessed changes in cell signaling after *FLCN* knockdown (Fig. 3A). After long-term *FLCN* knockdown, we observed marked alterations in the expression of genes involved in multiple pathways that have been previously linked to BHD: (i) upregulation of *HIF1A* [12] toward the gene targets *SLC2A2* (11.2-fold) and *DDIT4* (1.6-fold) and the dramatic reduction of *DEPTOR* (by 93%), the negative regulator of mTORC1. (ii) Increased expression of *TGF β* (2.1-fold



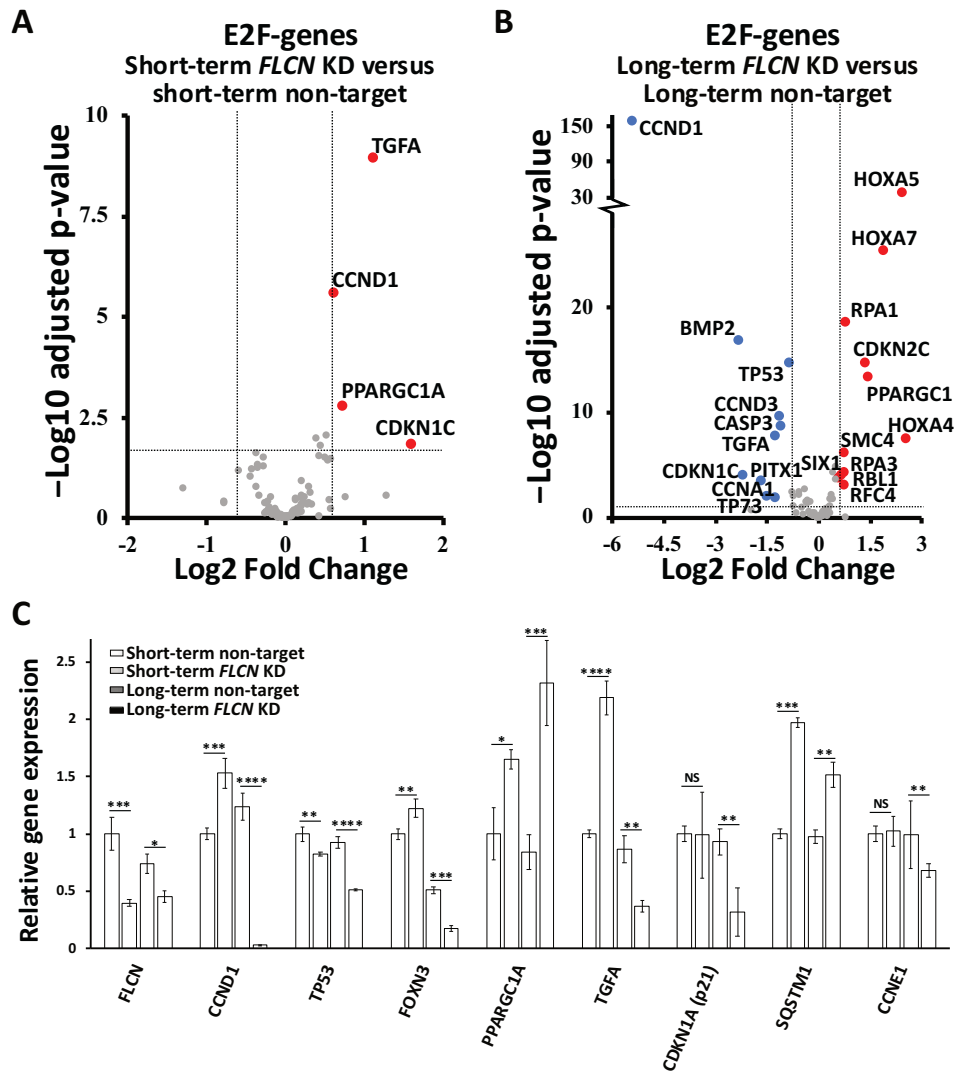


Fig. 2 Differentially expressed genes linked to E2F and known *FLCN* regulatory genes after *FLCN* knockdown. Differential gene expression of E2F genes was compared between **A** short-term *FLCN* knockdown cells and nontarget shRNA knockdown cells and **B** long-term *FLCN* knockdown and nontarget shRNA knockdown HK2 cells after RNA sequencing. Volcano plots are shown with the following thresholds: \leq & \geq 2.5-fold change and $\text{padj} < 0.05$ with false rate discovery (FDR) correction applied. **C** *FLCN*-linked genes from this RNA sequencing experiment are graphed and include *FLCN*, *CCND1*, *TP53*, *PPARGC1A*, *TGFA*, *CDKN1A*, *SQSTM1* and *CCNE1*.

increase) and SMAD3 (1.8-fold increase) was detected, suggesting elevated TGF β -SMAD signaling [28]. (iii) There was a 20% reduction in SIRT1 expression (a negative regulator of PPARGC1A), a marked 2.7-fold increase in PPARGC1A expression, and a subsequent increase in PPARGC1A-regulated genes, namely, *NR1H3*, *SOX9*, and *HMOX1* (>2.5-fold change and <0.0001 adjusted p value). This observation supports previously published work in which PPARGC1A was observed to drive mitochondrial biogenesis and metabolic transformation in BHD cell models [11]. More than half of the G₁/S regulatory genes were dysregulated following *FLCN* knockdown, with notable changes to (iv) INK4 family members that negatively regulate CCND1 (graphed in Fig. 3B, CDKN2A-D) and (v) cell cycle regulators that control RB1 phosphorylation and E2F activation. We also found evidence that *FLCN* knockdown cells employ feedback mechanisms to reduce the expression of G₁/S regulatory components. For example, although CCND1 was initially upregulated upon *FLCN* knockdown (Fig. 2C and Supplementary Fig. 4), CCND1 mRNA was strikingly downregulated by 97% after long-term *FLCN* knockdown (Figs. 2C and 3A). Given the bidirectional relationship between metabolism

and cell cycle progression [29], we speculate that the altered metabolism observed in *FLCN*-deficient cells [11, 12] could underlie the defects in E2F-regulated cell cycle gene expression that become more pronounced and protumorigenic over time.

To assess whether alterations in spheroid growth correlated with the observed alterations in cell cycle pathway dysregulation, we generated lysates from the spheroids shown in Fig. 1B and analyzed a panel of cell cycle proteins. We found that spheroids from long-term *FLCN* knockdown had elevated CCND1 protein expression and RB1 phosphorylation (Fig. 3C). These alterations after long-term *FLCN* knockdown could correlate with their increased growth properties. As negative regulators of cyclin:cyclin dependent kinase (CDK) complexes, we analyzed TP53 and cyclin-dependent kinase inhibitor 1A (CDKN1A, known as p21/WAF1). We found that these genes were highly expressed following *FLCN* knockdown, and in both cases, the levels were greater after long-term knockdown. These findings contrast with the RNA data, in which *CCND1*, *TP53* and *CDKN1A* mRNA expression was downregulated in response to long-term *FLCN* knockdown (Fig. 2C). Long-term *FLCN* knockdown also elevated the expression of β -catenin, which is associated with

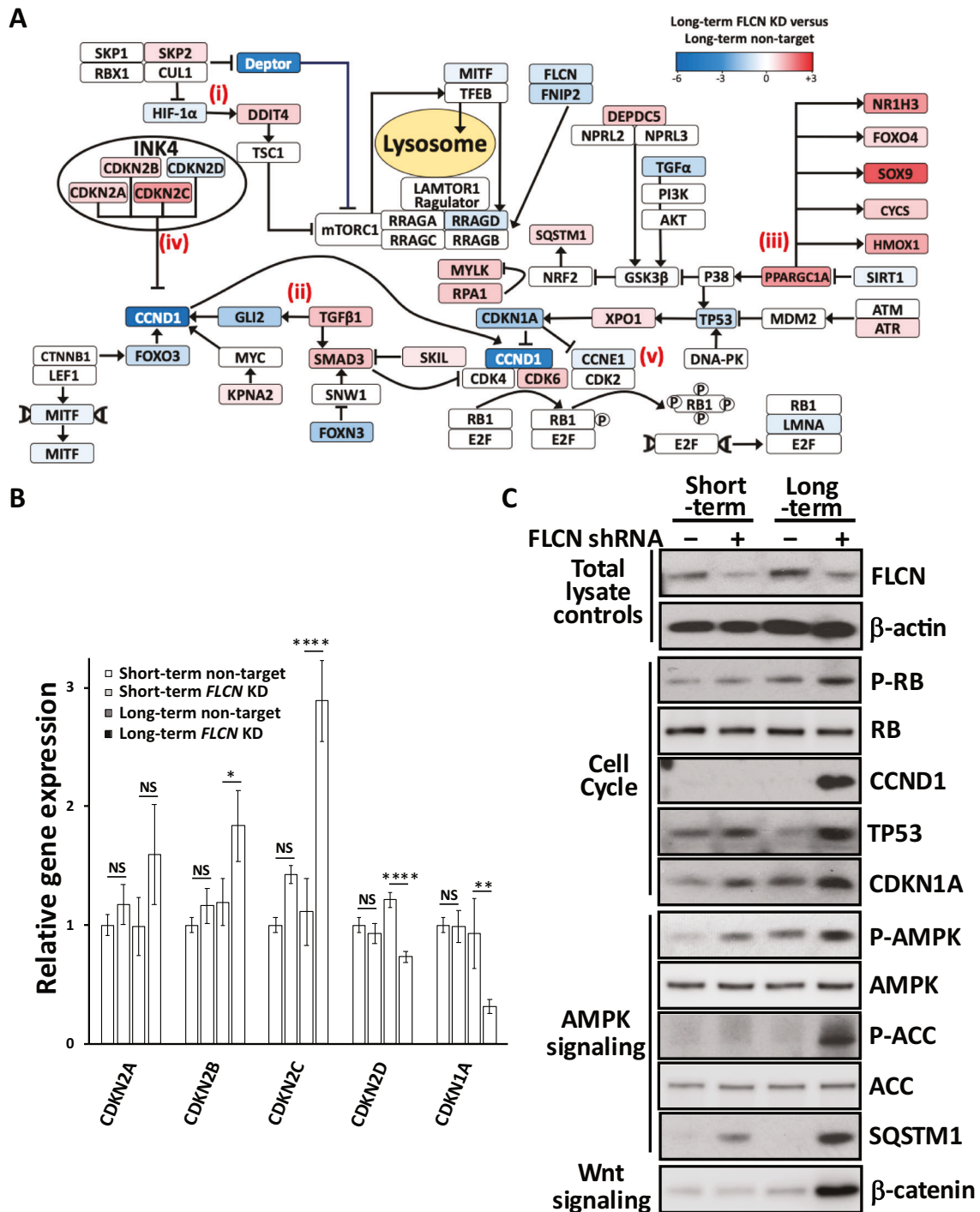


Fig. 3 Differentially expressed genes and their associated signaling pathways. **A** RNA sequencing was used to compare long-term *FLCN* shRNA-mediated knockdown and nontargeting shRNA-mediated knockdown in HK2 cells (scale is set to log₂-fold change). Each gene is depicted in a signaling flow diagram. The known signaling functions of *FLCN* include (i) enhancing HIF-1 α activity, as shown by increased expression of the HIF-1 α target genes *SLC2A2* and *REDD1*. A signaling feedback mechanism reduces HIF-1 α through reducing HIF-1 α expression and upregulating *SKP2*, a HIF-1 α inhibitor. (ii) Upregulation of TGF β /SMAD3 signaling upon knockdown of *FLCN*. SMAD3 is an inhibitor of the CCND1-CDK4/CDK6 complex. (iii) The expression of PGC1 α and its downstream genes *NR1H3*, *FOXO4*, *SOX9*, *CYCS*, and *HMOX1* was markedly upregulated upon *FLCN* knockdown. (iv) The *INK4* family members that inhibit CCND1 and *CDKN2A-C* are increased, while *CDKN2D* is reduced. (v) Reduced expression of *CDKN1A* inhibits both CCND1 and CCNE1 activity. This finding demonstrated the presence of a transcriptional feedback mechanism that enhances CDK4/6 and CDK2 activity. Further differences were observed with enhanced *CDK6* expression and decreased expression of *CCND1* and *CCNE1*. **B** Relative gene expression of cyclin-dependent kinase inhibitors across the different HK2 cell lines was calculated ($n = 3$). **C** Protein lysates from spheroids generated from HK2 cells with or without short- or long-term *FLCN* shRNA knockdown (nontargeted shRNA was used as a control) were probed for phosphorylated RB1, CCND1, TP53, and CDKN1A; phosphorylated AMPK; and ACC; SQSTM1, β -catenin, FLCN, and β -actin, which were used as loading controls ($n = 3$).

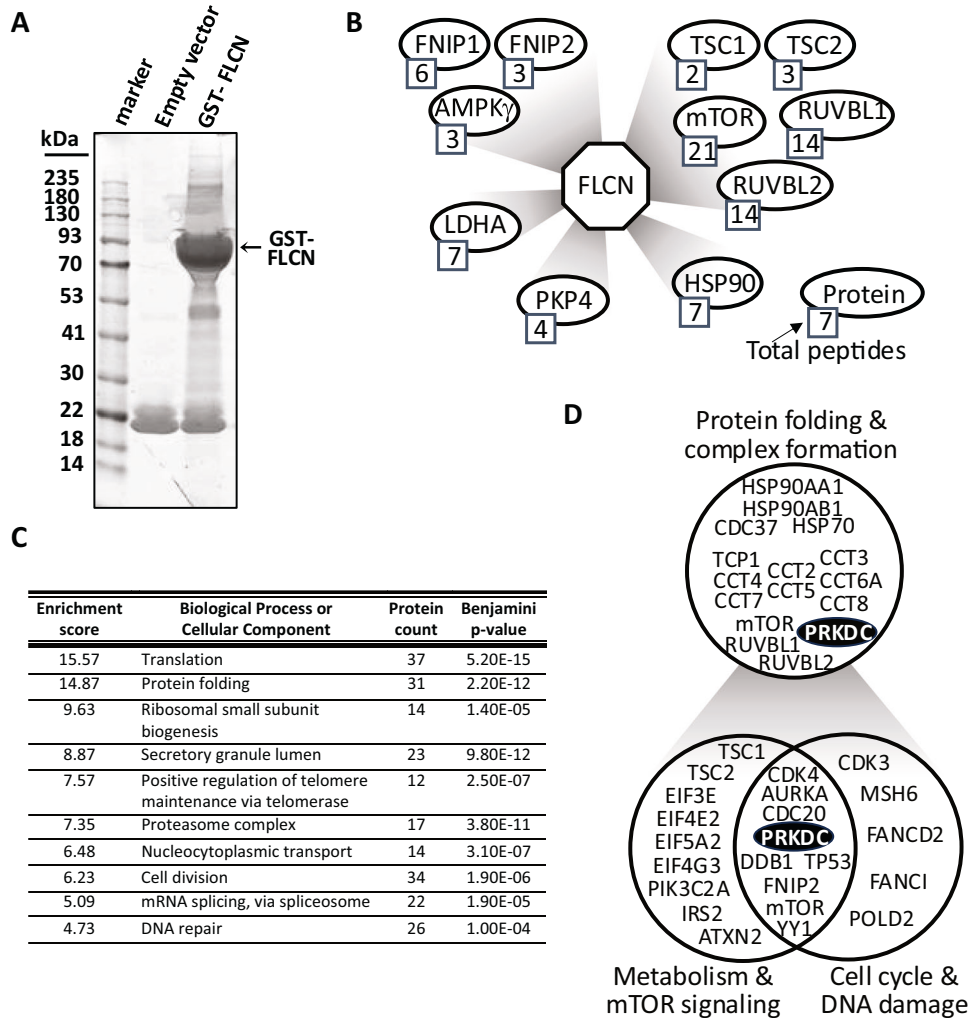


Fig. 4 **FLCN has an extensive PPI network.** **A** GST-FLCN was overexpressed in HEK293 cells, after which the purified and interacting proteins were separated via SDS-PAGE and stained with colloidal blue. The gel was sectioned for mass spectrometry analysis. **B** The FLCN protein interaction network is shown, which includes known FLCN interactions. The total peptide sequences identified after mass spectrometry are indicated. **C** FLCN-binding proteins identified by mass spectrometry were analyzed by DAVID, and the top ten enriched scored biological processes or cellular components are presented. **D** FLCN-binding proteins are involved in protein folding and complex formation, metabolism and mTOR signaling, and cell cycle and DNA damage.

increased WNT signaling, in line with our RNA sequencing findings (Fig. 1C). Sequestosome 1 (SQSTM1, also known as p62) mRNA was also increased by 1.5-fold (Fig. 2C), and protein expression was markedly enhanced (Fig. 3C). AMPK and acetyl-CoA carboxylase (ACC) phosphorylation was enhanced following *FLCN* knockdown and was more evident after long-term knockdown (Fig. 3C). High levels of SQSTM1 and AMPK activation are consistent with metabolic alterations and energy stress, as previously reported in BHD models [11].

FLCN interacts with components of the cell cycle and DDR

To further define FLCN as a tumor suppressor, mass spectrometry of GST-tagged FLCN-interacting partners was performed (Fig. 4A). This revealed 603 potential FLCN-binding proteins, and successful enrichment of FLCN-binding proteins was confirmed via the identification of previously characterized FLCN interactors, such as FLCN-interacting protein 1 (FNIP1) [30], FNIP2 [31], LDHA [13], PKP4 [14, 15] (Fig. 4B) and the BRCA1 A complex component BRE [32]. When considering identified interactors for which more than one unique peptide was identified, 541 potential FLCN-binding proteins were mapped to functional clusters by DAVID analysis (Fig. 4C). This

revealed that the strongest enrichment was in proteins involved in translation, in keeping with the known function of FLCN in the mTORC1 pathway. Interestingly, we identified protein folding chaperones as highly enriched in our dataset; these chaperones included all eight components of the TRiC/CCT chaperonin complex and two isoforms of HSP90 plus the co-chaperone CDC37. The chaperonin CCT helps fold both mLST8 and Raptor, which are part of mTORC1 [33], while the R2TP complex (which includes RUVBL1 and RUVBL2), together with heat shock protein 90 (HSP90), is a chaperone for the assembly of protein complexes, including phosphatidylinositol 3-kinase (PI3K)-like kinases (PIKKs), such as TOR and PRKDC (referred to as DNA-dependent protein kinase (DNA-PK)) (highlighted in Figs. 4B and 4D) [34]. Additionally, FLCN was previously described as an HSP90 client protein, where the HSP90-FLCN interaction enhances the stability of FLCN, while the FLCN binding partners FNIP1/FNIP2 function as co-chaperones [35]. Several CCT substrates are cell cycle proteins, particularly those involved in the G₁/S phase (discussed in [36]), so it was interesting to observe that cell division was also one of the top 10 enriched processes (Fig. 4C). There was a greater proportion of FLCN-binding proteins linked to the G₁/S phase in the different stages of the cell cycle

(Supplementary Fig. 3A), including CDK1, CDC20, TP53 and RB-binding protein 7 (RBBP-7). These findings support our RNA sequencing findings, indicating that FLCN is linked to the G₁/S phase of the cell cycle. One cell cycle protein, DNA-PK, was our top interactor, with the most peptides identified (Supplementary Fig. 3B). This protein also plays a role in DNA repair, another process enriched in our interactome (Fig. 4C). Indeed, a number of interactors were involved in metabolism, the cell cycle and DNA damage (Fig. 4D).

DNA-PK interacts with FLCN

As our top interactor, with 66 unique peptides and 17.9% coverage (Supplementary Fig. 3B, C), we focused our attention on DNA-PKs. DNA-PKs plays an important role in cell cycle check point control during DNA damage [37], so this aligns with our transcriptomic work linking FLCN to cell cycle dysregulation (Fig. 2B) and the finding of DNA-PK in our FLCN interaction network (Fig. 4D). Given that there are limitations to overexpressed protein purification methods, i.e., potential nonspecific or artificial protein binding to either beads or mislocalized overexpressed proteins, we carried out further FLCN-binding validation experiments on DNA-PKs. We initially examined whether endogenous DNA-PKs copurified with GST-tagged FLCN (Fig. 5A). We observed a robust interaction between DNA-PKs and GST-FLCN but not between DNA-PKs and the empty vector control, revealing that there was no nonspecific binding of DNA-PKs to the beads. The other PIKK family members, ATM and ATR, were not immunoprecipitated with FLCN. After further validating the DNA-PKs interaction, we observed the interaction of endogenous DNA-PKs with immunoprecipitated endogenous FLCN (Fig. 5B). Next, we compared the associations of DNA-PKs with wild-type FLCN and the BHD patient-derived mutants Y463X and H429X (Fig. 5C). Both C-terminal truncation mutants of FLCN interacted with endogenous DNA-PKs. We then considered that FLCN might be a direct substrate of DNA-PKs. Therefore, *in vitro* DNA-PK kinase assays were performed using TP53 as a DNA-PK substrate control (Fig. 5D). Supplementation with dsDNA was used to further enhance the kinase activity of DNA-PK. Unlike that of TP53, where DNA-PK-mediated phosphorylation was enhanced with the supplementation of dsDNA, we observed a much weaker level of [³²P]-incorporation into FLCN. Neither FNIPI nor FNIPI2 further enhanced this low level of phosphorylation (data not shown). Given the low levels of [³²P]-incorporation into FLCN, which was not further enhanced by supplementation with dsDNA, FLCN is unlikely to be a direct substrate of DNA-PK in these assays.

Cell cycle progression is dysregulated following long-term loss of FLCN

As DNA-PKs regulates the phosphorylation of H2AX in response to cell cycle progression and DNA damage [38], we next analyzed γ H2AX (H2AX phosphorylated at Ser139). Following short-term FLCN knockdown, γ H2AX expression was enhanced, and long-term FLCN knockdown significantly elevated γ H2AX expression (Fig. 6A and Supplementary Fig. 4A). γ H2AX is classically regarded as a marker of DNA damage involved in the surveillance and repair of double strand breaks, such as those induced by ionizing radiation (IR). However, γ H2AX has also been reported to occur independently of double-strand DNA breaks [39], in mitotic cells [38] and in response to serum starvation [40]. Therefore, we next assessed the interaction between DNA-PKs and GST-FLCN following IR and found that endogenous DNA-PKs dissociated from GST-FLCN after IR treatment at 5 and 10 Gy (Fig. 6B). This finding revealed that the FLCN/DNA-PK interaction is regulated by DNA damage. DNA damage markers in 5 Gy IR-treated cells were analyzed to determine whether FLCN knockdown altered DDR signaling. IR enhanced γ H2AX expression, as expected, as indicated by increased basal and IR-induced γ H2AX expression in FLCN-deficient HK2 cells (Fig. 6C). DNA-PKs autophosphorylation is essential for the appropriate regulation of DNA strand end processing, enzyme inactivation, and complex dissociation from

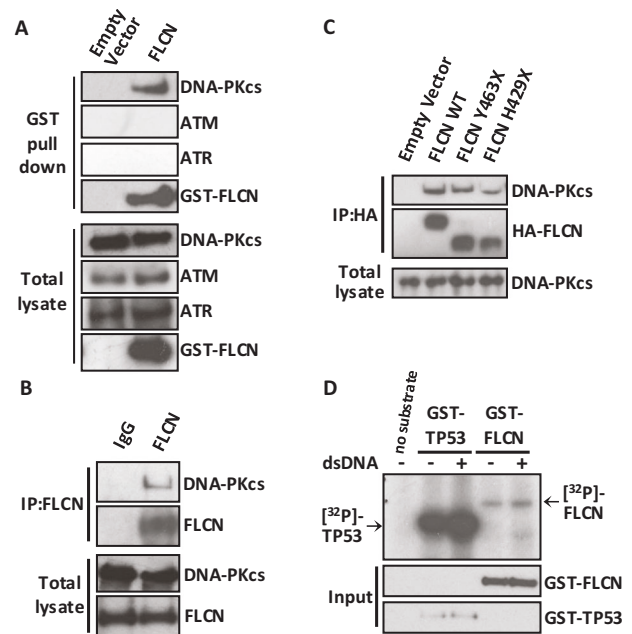


Fig. 5 FLCN interacts with DNA-PK. **A** GST-tagged FLCN was overexpressed in HEK293 cells and used as a bait protein to validate the interactions between FLCN and endogenously expressed DNA damage components (DNA-PKs, ATM, and ATR) via GST pull-down. **B** Endogenous FLCN was immunoprecipitated using an antibody against N-terminal FLCN, and the interaction of endogenous DNA-PKs was detected via western blotting. **C** HA-tagged FLCN constructs (wild-type FLCN (WT)) and two patient-derived C-terminal truncation mutants (Y463X and H429X) were overexpressed in HEK293 cells and immunoprecipitated using anti-HA antibodies, and bound endogenous DNA-PKs was detected via western blotting. **D** DNA-PK kinase assays were performed using GST-FLCN or GST-TP53, which were overexpressed and purified from HEK293 cells. The incorporation of radiolabeled phosphate [³²P] was determined with active DNA-PK, which was further induced by supplementation with short double-stranded DNA (dsDNA).

DNA (see review [41]). However, no change in DNA-PK autophosphorylation was observed upon FLCN knockdown. While phosphorylation of TP53 at Ser15 was induced under IR, there was no difference between FLCN knockdown and wild-type cells (Fig. 6C). These data showed that although γ H2AX is elevated following FLCN loss, FLCN loss has no direct impact on IR-induced DNA-PK signaling; i.e., elevated γ H2AX is unlikely to be reflective of double-strand DNA breaks. When the RNA sequencing data with and without FLCN knockdown were analyzed through Mutect2, there was no evidence of enhanced DNA mutation (data not shown). This finding indicates that FLCN loss is unlikely to enhance DNA damage but might be related to cell cycle control linked to DNA-PK.

To determine whether cell cycle defects following FLCN loss are linked to the G₁/S phase transition in mammalian cells, we examined the expression of CCND1 in HK2 cells following IR treatment (Fig. 6C). CCND1 expression was greater after FLCN was knocked down, which is in line with the findings of previous work [17]. After long-term FLCN knockdown, CCND1 protein expression further increased (Fig. 6C), even though CCND1 mRNA was substantially reduced (Supplementary Fig. 4B). In healthy cells, CCND1 protein levels are typically reduced after IR as part of a normal DNA damage cell cycle checkpoint control mechanism [41]. However, in FLCN knockdown cells following IR treatment, CCND1 protein levels remain elevated, indicating a defect in the normal control of CCND1 after DNA damage (Fig. 6C). Additional HK2 clones with FLCN knockdown showed higher levels of CCND1

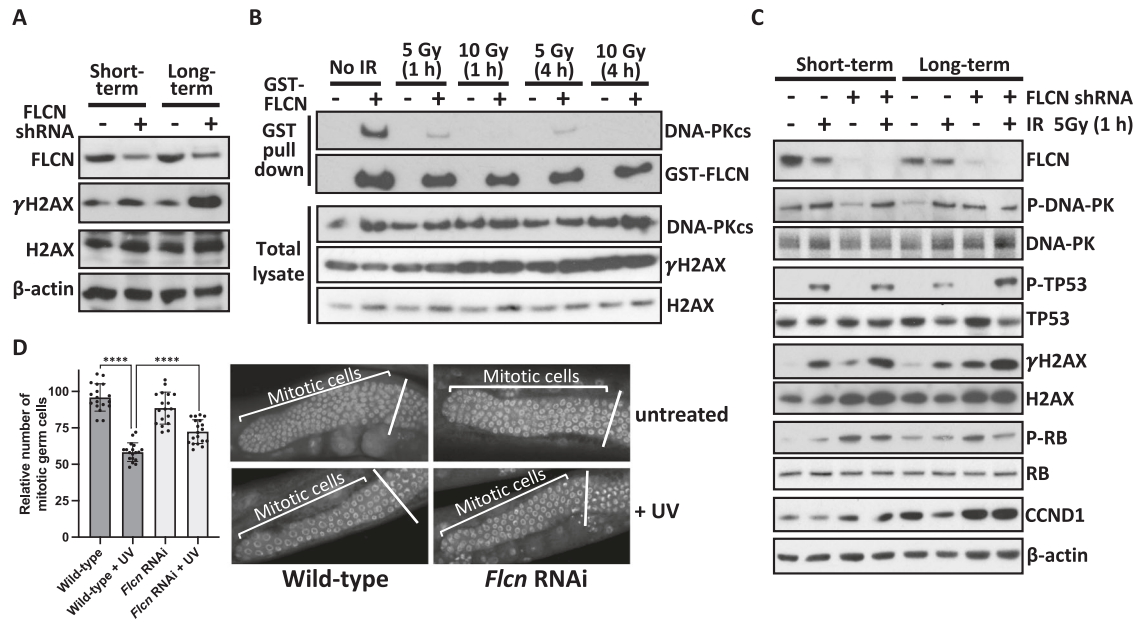


Fig. 6 *FLCN* knockdown promotes cell cycle progression. **A** Serine 139 phosphorylation of the histone variant H2AX (γ H2AX) was assessed under basal conditions in HK2 cells grown in standard cell culture with and without short-term or long-term *FLCN* shRNA knockdown (nontargeted shRNA was used as a control). **B** The *FLCN*/DNA-PKcs interaction was investigated following IR-induced DNA damage. GST-tagged *FLCN* was overexpressed in HEK293 cells that were then subjected to IR (5 or 10 Gy) and left for either 1 or 4 h prior to cellular lysis, as indicated. GST-*FLCN* was purified, and endogenous DNA-PKcs was detected via western blotting. **C** In HK2 cells with or without short- or long-term *FLCN* shRNA knockdown, DNA damage markers were assessed following 5 Gy IR for 1 h, where indicated. γ H2AX, P-DNA-PKcs (Ser2056) and the downstream DNA-PK substrate P-TP53 (Ser15) are shown. G_1/S phase cell cycle markers CCND1 and P-RB1 were analyzed and *FLCN* and β -actin were used as controls. **D** Mitotic germ cells were quantified in *C. elegans* with and without *Flcn* siRNA knockdown and subjected to UV damage, where indicated. Mitotic germ cells were scored and graphed. Representative images of the mitotic cells are presented ($n = 18$).

when compared to control HK2 cells (Supplementary Fig. 4C). Increased RB1 phosphorylation was also observed after *FLCN* knockdown, implying an increase in the number of active G_1/S cyclin-CDK complexes (Fig. 6C). RB1 phosphorylation leads to E2F activation and entry into S phase, suggesting that knockdown of *FLCN* favors G_1/S checkpoint slippage. In support of this observation, transcriptomic analysis revealed enrichment of E2F-regulated genes in *FLCN*-knockdown HK2 cells (Fig. 2B).

To examine the role of *FLCN* in an alternative system, we analyzed *C. elegans* with and without *Flcn* RNAi knockdown. *C. elegans* has previously been used as a model organism to characterize the effects of DNA damage and cell cycle checkpoint control in germ cells (reviewed in [42]). While we observed no change in the relative number of mitotic germ cells upon *Flcn* knockdown, *Flcn*-knockdown worms were defective in cell cycle arrest caused by UV-induced DNA damage. We observed a small increase in the relative number of mitotic germ cells after UV irradiation (Fig. 6D). These findings support the hypothesis that *Flcn* knockdown results in dysregulation of cell cycle progression following DNA damage. Overall, *FLCN* knockdown leads to cell cycle dysregulation with and without DNA damage, where we observed heightened levels of CCND1 and RB1 phosphorylation as well as enhanced E2F-mediated transcription of S-phase genes.

DISCUSSION

Despite the germline *FLCN* mutation, RCC takes several decades to develop in BHD patients, but most studies to date have analyzed only the immediate impact of *FLCN* loss in cells. Therefore, we explored the long-term consequences of *FLCN* loss through transcriptomic and proteomic analysis to better characterize *FLCN* as a tumor suppressor and, in doing so, uncovered links to DNA-PK and cell cycle control.

Proteomic analysis revealed that *FLCN* interactors are involved in protein folding, the cell cycle and DNA repair, including DNA-PKs. DNA-PKs showed strong binding to both wild-type and BHD patient-derived *FLCN* mutants. Arguing against a nonspecific binding artifact, this interaction was completely reversed under IR. DNA-PK plays a key role in the DNA damage response. *FLCN* loss was previously linked to DNA damage, where *FLCN*-deficient cells were shown to be sensitive to PARP inhibitors due to impairment of the DNA repair ability associated with the BRCA1 complex [32]. In our study, we detected the BRCA1 A complex member BRE in our *FLCN* pull-down experiments and observed that long-term *FLCN* knockdown resulted in an increase in γ H2AX. We believe that this increase in γ H2AX expression is unlikely to be due to DNA damage, as other markers of DNA repair signaling were unaltered. DNA-PKs play roles beyond the DNA damage response, including in cell cycle progression [43]; therefore, we propose that *FLCN* loss causes defects in cell cycle control. It is likely that the higher levels of γ H2AX after *FLCN* knockdown reflect the known role of DNA-PK in enhancing γ H2AX expression during cell cycle control, which can occur independently of DNA damage [43]. Therefore, the large transcriptional changes in cell cycle genes observed upon *FLCN* knockdown are likely due to epigenetic alterations or altered gene expression downstream of metabolic signaling changes rather than an accumulation of unrepaired DNA errors.

While our study specifically focused on the G_1/S phase of the cell cycle, it should be noted that *FLCN* has also been linked to the G_2/M phase [44]. Upon *FLCN* knockdown, we observed aberrant protein expression of CCND1. Previous work revealed that the translation of CCND1 mRNA was negatively regulated by a *FLCN* regulatory cis-acting element in its 3'-untranslated region [17], which partially helps to explain why CCND1 protein levels increase upon *FLCN*-deficiency. We observed that CCND1 protein levels remained elevated even after IR-induced DNA damage in the absence of *FLCN*, suggesting that the control of DNA damage at

the cell cycle checkpoint may be compromised by FLCN knockdown. As RB1 phosphorylation was elevated upon FLCN knockdown, there must be a higher level of CDK activity toward RB1 in these cells. Analysis of the RNA sequencing data provided further evidence of RB1/E2F activation, as E2F target genes were more highly expressed in the absence of FLCN. Furthermore, upon FLCN knockdown, we observed a modest reduction in the G₁ population of cells, suggesting a potential increase in proliferative drive through G₁/S in the absence of FLCN. The high protein levels of CCND1 and RB1 hyperphosphorylation in long-term FLCN-knockdown HK2 tumor spheroids likely contributed to their observed tumorigenicity.

Our interactome data and enrichment of protein folding chaperones are consistent with previous observations that FLCN is folded and assembled into large multiprotein complexes. Recent publications, such as the FLCN-FNIP2-Rag-Ragulator complex [45] and the mTORC1-TFEB-Rag-Ragulator mega-complex, which includes the FLCN-regulated RagC [46], have shown that FLCN is involved in mega-complexes that control metabolism.

While a limitation of this work is that our cell line data is restricted to the HK2 cell line due to the resources required for long-term culturing, we also used a *C. elegans* model to further confirm that FLCN is connected to cell cycle control. The DDR pathway is defined by several key features, one of which is cell cycle checkpoint control, which is regulated by DNA-PK. This helps prevent the propagation of somatic mutations into progeny cells when DNA damage is present and not repaired. Two pieces of evidence indicate a defect in proper cell cycle checkpoint control upon FLCN loss. First, *C. elegans* animals with *Fln* knockdown had more mitotic germ cells following DNA damage than did those with nontarget *Fln* knockdown. Second, in mammalian HK2 cells, CCND1/RB1-P remained elevated in the presence of DNA damage when FLCN was knocked down, while this checkpoint was engaged normally in wild-type cells (as observed by reduced CCND1/RB1 phosphorylation). Further studies in additional cell models and systems would help confirm and expand these findings to explain whether such dysregulation of cell cycle occurs over time and drives earlier onset of cancer progression observed in BHD patients.

MATERIALS AND METHODS

Cell culture

Unless stated otherwise, laboratory reagents were purchased from Merck Millipore (Burlington, Massachusetts, USA). HEK293 cells were purchased from American Type Culture Collection (Manassas, Virginia, USA). Cell maintenance and the generation of stable FLCN-knockdown HK2 cells have been described previously [10] and all clones were confirmed to match the HK2 line by STR analysis and knockdown clones remained stable in culture (outsourced to Northgene, Deeside, UK). Short- and long-term knockdown were defined as < 30 and > 105 passages after clonal selection, respectively. Lipofectamine 2000 transfection was carried out according to the manufacturer's protocol (Life Technologies, Paisley, UK). Irradiation (IR) was carried out using a Gammacell 1000 Elite (Nordion Gamma Technologies, Abingdon, UK). The cells were checked with a Venor™ GeM Advance Mycoplasma Detection Kit (Minerva Biolabs, Berlin, Germany) according to the manufacturer's guidelines and were found to be mycoplasma negative. Tumor spheroid growth assays in soft agar were performed as previously described [47]. For spheroid protein analysis, 12,500 cells were allowed to self-aggregate in 1.5% (w/v) agarose-coated wells. Forty-eight spheroids per cell line were lysed in 1x sample buffer (62.8 mM Tris, 10% (v/v) glycerol, 2% (w/v) SDS, 0.1% (w/v) bromophenol blue, 50 mM dithiothreitol (DTT) added just before use), sonicated and boiled prior to blotting. Cell lysis and western blot analysis were performed as previously described [48].

Antibodies

Unless otherwise specified, the antibodies used were purchased from Cell Signaling Technology (Danvers, MA, USA). The phospho-specific antibodies used included p-H2AX Ser139 (#9718 P (20E3)), p-TP53 Ser15 (#9286 P (16G8)), p-RB1 Ser780 (D59B7), p-AMPK Thr172 (#2531), p-ACC Ser79 (#3661) and p-

DNA-PK Ser2056 (ab124918 from Abcam Plc., Cambridge, UK). The pan-antibodies used included β-actin (#84573 (D6A8)), CCND1 (#2922), CDKN1A (12D1), SQSTM1 (#5114), and TP53 (DO-1 from Bethyl Laboratories Ltd., Montgomery, TX, USA) and from Merck Millipore both GST (#DAM1411332), ATM (#2873 (D2E2)), ATR (#2790), DNA-PKcs (#D00148436), and HA (#1186742300 from Roche Products Limited, Welwyn Garden City, UK). The custom-made N-terminal anti-FLCN was previously described [10].

GST pull-down and coimmunoprecipitation assays

HEK293 cells were transfected with either GST-FLCN in the pDEST27 backbone (Life Technologies, 11812013) or the pcDNA3 empty vector. Then, 150 μL of lysate was incubated with preblocked glutathione-Sepharose 4B beads (GE Healthcare, Chalfont St. Giles, UK) at 4°C in a rotary shaker for 3 h. The beads were washed 5 times in BHD lysis buffer [8] supplemented with 300 mM NaCl for DNA-PKcs (250 mM for all other proteins). The bound proteins were eluted using 10 mM glutathione in elution buffer (20 mM HEPES (pH 8), 200 mM NaCl, 5 mM MgCl₂) to avoid elution and subsequent detection of proteins that bound nonspecifically to the beads. The eluent was mixed with NuPAGE LDS sample buffer containing 100 mM DTT. For coimmunoprecipitation, HEK293 cells were transfected with HA-FLCN wild type, HA-FLCN Y463X or HA-FLCN H429X in the pcDNA3.1 vector or pcDNA3.1 empty vector (described in [8]). The lysates were precleared with unblocked protein G-Sepharose beads (GE Healthcare) for 1 h at 4°C and then centrifuged for 3 min at 3000 rpm and 4°C to remove the beads. The lysates were then incubated with anti-HA antibodies for 2 h at 4°C in a rotary shaker before BSA-blocked protein G-Sepharose beads were added for 2 h. The beads were subsequently washed, and the proteins were dissociated with sample buffer containing 25 mM DTT at 70°C for 10 min.

Mass spectrometry sample preparation, sequencing, and FLCN protein–protein interaction analysis

Proteins were identified from gel fragments by liquid chromatography-tandem mass spectrometry (LC–MS/MS), as previously described [49]. The identified proteins were filtered by removal of keratins. Proteins with 2 or more unique peptides identified were analyzed using the Database for Annotation, Visualization and Integrated Discovery (DAVID) Functional Annotation Clustering [50]. Known FLCN interactors were screened manually using the following GO terms: (i) protein folding GO:0006457, (ii) metabolic processes GO:0031323, (iii) cell cycle GO:0007049 and (iv) response to DNA damage GO:0006974.

Statistical analysis

Unless stated otherwise, after determining a normal (Gaussian) distribution (Shapiro–Wilk test), ordinary one-way ANOVA with Tukey's multiple comparisons was carried out using Prism GraphPad; * $p < 0.05$, ** $p < 0.01$, *** $p < 0.001$, **** $p < 0.0001$, and not significant (ns). All the data are presented as the mean ± SEM. Experiments were repeated 3 times as biological repeats, unless stated otherwise. Figure legends state n -numbers and statistical analysis if different to the above. No inclusion or exclusion criteria, randomization or blinding of experiments were carried out for either the cell line and *C. elegans* experiments.

DATA AVAILABILITY

Proteomic dataset is available at <https://doi.org/10.6084/m9.figshare.25943011>. RNA sequencing data is available at Gene Expression Omnibus, accession GSE283021.

REFERENCES

- Birt AR, Hogg GR, Dubé WJ. Hereditary multiple fibrofolliculomas with trichodiscomas and acrochordons. *Arch Dermatol.* 1977;113:1674–7.
- Schmidt LS, Linehan WM. Molecular genetics and clinical features of Birt-Hogg-Dubé syndrome. *Nat Rev Urol.* 2015;12:558–69.
- Johannesma PC, van de Beek I, van der Wel TJWT, Reinhard R, Rozendaal L, Starink TM, et al. Renal imaging in 199 Dutch patients with Birt-Hogg-Dubé syndrome: Screening compliance and outcome. *PLoS ONE.* 2019;14:e0212952.
- Li K, Wada S, Gosis BS, Thorsheim C, Loose P, Arany Z. Folliculin promotes substrate-selective mTORC1 activity by activating RagC to recruit TFE3. *PLoS Biol.* 2022;20:e3001594.
- Napolitano G, Di Malta C, Esposito A, de Araujo MEG, Pece S, Bertalot G, et al. A substrate-specific mTORC1 pathway underlies Birt-Hogg-Dubé syndrome. *Nature.* 2020;585:597–602.

6. Meng J, Ferguson SM. GATOR1-dependent recruitment of FLCN-FNIP to lysosomes coordinates Rag GTPase heterodimer nucleotide status in response to amino acids. *J Cell Biol.* 2018;217:2765–76.
7. Di Malta C, Zampelli A, Granieri L, Vilardo C, De Cegli R, Cinque L, et al. TFE3 and TFE3 drive kidney cystogenesis and tumorigenesis. *EMBO Mol Med.* 2023;15:e16877.
8. Dunlop EA, Seifan S, Claessens T, Behrends C, Kamps MA, Rozycka E, et al. FLCN, a novel autophagy component, interacts with GABARAP and is regulated by ULK1 phosphorylation. *Autophagy.* 2014;10:1749–60.
9. Paquette M, El-Houjeiri L, C Zirten L, Puustinen P, Blanchette P, Jeong H, et al. AMPK-dependent phosphorylation is required for transcriptional activation of TFE3 and TFE3. *Autophagy.* 2021;17:3957–75.
10. Luijten MN, Basten SG, Claessens T, Vernooij M, Scott CL, Janssen R, et al. Birt-Hogg-Dube syndrome is a novel ciliopathy. *Hum Mol Genet.* 2013;22:4383–97.
11. Yan M, Gingras MC, Dunlop EA, Nouët Y, Dupuy F, Jalali Z, et al. The tumour suppressor folliculin regulates AMPK-dependent metabolic transformation. *J Clin Invest.* 2014;124:2640–50.
12. Preston RS, Philp A, Claessens T, Gijzen L, Dydensborg AB, Dunlop EA, et al. Absence of the Birt-Hogg-Dubé gene product is associated with increased hypoxia-inducible factor transcriptional activity and a loss of metabolic flexibility. *Oncogene.* 2011;30:1159–73.
13. Woodford MR, Baker-Williams AJ, Sager RA, Backe SJ, Blanden AR, Hashmi F, et al. The tumor suppressor folliculin inhibits lactate dehydrogenase A and regulates the Warburg effect. *Nat Struct Mol Biol.* 2021;28:662–70.
14. Medvetz DA, Khabibullin D, Hariharan V, Ongusaha PP, Goncharova EA, Schlechter T, et al. Folliculin, the product of the Birt-Hogg-Dube tumour suppressor gene, interacts with the adherens junction protein p0071 to regulate cell-cell adhesion. *PLoS ONE.* 2012;7:e47842.
15. Nahorski MS, Seabra L, Straatman-Iwanowska A, Wingenfeld A, Reiman A, Lu X, et al. Folliculin interacts with p0071 (plakophilin-4) and deficiency is associated with disordered RhoA signalling, epithelial polarization and cytokinesis. *Hum Mol Genet.* 2012;21:5268–79.
16. Gaur K, Li J, Wang D, Dutta P, Yan SJ, Tsurumi A, et al. The Birt-Hogg-Dubé tumour suppressor Folliculin negatively regulates ribosomal RNA synthesis. *Hum Mol Genet.* 2013;22:284–99.
17. Kawai A, Kobayashi T, Hino O. Folliculin regulates cyclin D1 expression through cis-acting elements in the 3' untranslated region of cyclin D1 mRNA. *Int J Oncol.* 2013;42:1597–604.
18. Laviolette LA, Mermoud J, Calvo IA, Olson N, Boukhali M, Steinlein OK, et al. Negative regulation of EGFR signalling by the human folliculin tumour suppressor protein. *Nat Commun.* 2017;8:15866.
19. van de Beek I, Glykofridis IE, Oosterwijk JC, van den Akker PC, Diercks GFH, Bolling MC, et al. PRDM10 directs FLCN expression in a novel disorder overlapping with Birt-Hogg-Dubé syndrome and familial lipomatosis. *Hum. Mol. Genet.* 2023;32:1223–35.
20. Schmidt LS, Vocke CD, Ricketts CJ, Blake Z, Choo KK, Nielsen D, et al. PRDM10 RCC: A Birt-Hogg-Dubé-like syndrome associated with lipoma and highly penetrant, aggressive renal tumors morphologically resembling type 2 papillary renal cell carcinoma. *Urology.* 2023;179:58–70.
21. Fukagawa A, Hama N, Totoki Y, Nakamura H, Arai Y, Saito-Adachi M, et al. Genomic and epigenomic integrative subtypes of renal cell carcinoma in a Japanese cohort. *Nat Commun.* 2023;14:8383.
22. Chen J, Futami K, Petillo D, Peng J, Wang P, Knol J, et al. Deficiency of FLCN in mouse kidney led to development of polycystic kidneys and renal neoplasia. *PLoS ONE.* 2008;3:e3581.
23. Hudon V, Sabourin S, Dydensborg AB, Kottis V, Ghazi A, Paquet M, et al. Renal tumour suppressor function of the Birt-Hogg-Dubé syndrome gene product folliculin. *J Med Genet.* 2010;47:182–9.
24. Jikuya R, Johnson TA, Maejima K, An J, Ju YS, Lee H, et al. Comparative analyses define differences between BHD-associated renal tumour and sporadic chromophobe renal cell carcinoma. *EBioMedicine.* 2023;92:104596.
25. Bracken AP, Ciro M, Cocito A, Helin K. E2F target genes: unraveling the biology. *Trends Biochem Sci.* 2004;29:409–17.
26. Harper JW, Adami GR, Wei N, Keyomarsi K, Elledge SJ. The p21 Cdk-interacting protein Cip1 is a potent inhibitor of G1 cyclin-dependent kinases. *Cell.* 1993;75:805–16.
27. Huot G, Vernier M, Bourdeau V, Doucet L, Saint-Germain E, Gaumont-Leclerc MF, et al. CHES1/FOXN3 regulates cell proliferation by repressing PIM2 and protein biosynthesis. *Mol Biol Cell.* 2014;25:554–65.
28. Cash TP, Gruber JJ, Hartman TR, Henske EP, Simon MC. Loss of the Birt-Hogg-Dubé tumour suppressor results in apoptotic resistance due to aberrant TGFβ-mediated transcription. *Oncogene.* 2011;30:2534–46.
29. Diehl FF, Sapp KM, Vander Heiden MG. The bidirectional relationship between metabolism and cell cycle control. *Trends Cell Biol.* 2024;34:136–49.
30. Baba M, Hong SB, Sharma N, Warren MB, Nickerson ML, Iwamatsu A, et al. Folliculin encoded by the BHD gene interacts with a binding protein, FNIP1, and AMPK, and is involved in AMPK and mTOR signaling. *Proc Natl Acad Sci USA.* 2006;103:15552–7.
31. Hasumi H, Baba M, Hong SB, Hasumi Y, Huang Y, Yao M, et al. Identification and characterization of a novel folliculin-interacting protein FNIP2. *Gene.* 2008;415:60–7.
32. Zhang Q, Xu Y, Zhang Z, Li J, Xia Q, Chen Y. Folliculin deficient renal cancer cells exhibit BRCA1 A complex expression impairment and sensitivity to PARP1 inhibitor olaparib. *Gene.* 2021;769:145243.
33. Cuéllar J, Ludlam WG, Tensmeyer NC, Aoba T, Dhavale M, Santiago C, et al. Structural and functional analysis of the role of the chaperonin CCT in mTOR complex assembly. *Nat Commun.* 2019;10:2865.
34. Seraphim TV, Nano N, Cheung YWS, Aluksanasuwan S, Colleti C, Mao YQ, et al. Assembly principles of the human R2TP chaperone complex reveal the presence of R2T and R2P complexes. *Structure.* 2022;30:156–71.
35. Woodford MR, Dunn DM, Blanden AR, Capriotti D, Loiseau D, Prodromou C, et al. The FNIP co-chaperones decelerate the Hsp90 chaperone cycle and enhance drug binding. *Nat Commun.* 2016;7:12037.
36. Dekker C, Stirling PC, McCormack EA, Filmore H, Paul A, Brost RL, et al. The interaction network of the chaperonin CCT. *EMBO J.* 2008;27:1827–39.
37. Yue X, Bai C, Xie D, Ma T, Zhou PK. DNA-PKcs: a multi-faceted player in DNA damage response. *Front Genet.* 2020;11:607428.
38. An J, Huang YC, Xu QZ, Zhou LJ, Shang ZF, Huang B, et al. DNA-PKcs plays a dominant role in the regulation of H2AX phosphorylation in response to DNA damage and cell cycle progression. *BMC Mol Biol.* 2010;11:18.
39. Revet I, Feeney L, Bruguera S, Wilson W, Dong TK, Oh DH, et al. Functional relevance of the histone gammaH2Ax in the response to DNA damaging agents. *Proc Natl Acad Sci USA.* 2011;108:8663–7.
40. Lu C, Shi Y, Wang Z, Song Z, Zhu M, Cai Q, et al. Serum starvation induces H2AX phosphorylation to regulate apoptosis via p38 MAPK pathway. *FEBS Lett.* 2008;582:2703–8.
41. Agami R, Bernards R. Distinct initiation and maintenance mechanisms cooperate to induce G1 cell cycle arrest in response to DNA damage. *Cell.* 2000;102:55–66.
42. Stergiou L, Hengartner MO. Death and more: DNA damage response pathways in the nematode *C. elegans*. *Cell Death Differ.* 2004;11:21–8.
43. Tu WZ, Li B, Huang B, Wang Y, Liu XD, Guan H, et al. γH2AX foci formation in the absence of DNA damage: mitotic H2AX phosphorylation is mediated by the DNA-PKcs/CHK2 pathway. *FEBS Lett.* 2013;587:3437–43.
44. Laviolette LA, Wilson J, Koller J, Neil C, Hulick P, Rejtar T, et al. Human folliculin delays cell cycle progression through late S and G2/M-phases: effect of phosphorylation and tumor associated mutations. *PLoS ONE.* 2013;8:e66775.
45. Shen K, Rogala KB, Chou HT, Huang RK, Yu Z, Sabatini DM. Cryo-EM Structure of the Human FLCN-FNIP2-Rag-Ragulator Complex. *Cell.* 2019;179:1319–29.
46. Cui Z, Napolitano G, de Araujo MEG, Esposito A, Monfregola J, Huber LA, et al. Structure of the lysosomal mTORC1-TFEB-Rag-Ragulator megacomplex. *Nature.* 2023;614:572–9.
47. Champion JD, Dodd KM, Lam HC, Alzahrani MAM, Seifan S, Rad E, et al. Drug inhibition of redox factor-1 restores hypoxia-driven changes in tuberous sclerosis complex 2 deficient cells. *Cancers.* 2022;14:6195.
48. Dunlop EA, Hunt DK, Acosta-Jaquez HA, Fingar DC, Tee AR. ULK1 inhibits mTORC1 signaling, promotes multisite Raptor phosphorylation and hinders substrate binding. *Autophagy.* 2011;7:737–47.
49. Doubleday PF, Ballif BA. Developmentally-dynamic murine brain proteomes and phosphoproteomes revealed by quantitative proteomics. *Proteomes.* 2014;2:197–207.
50. Sherman BT, Hao M, Qiu J, Jiao X, Baseler MW, Lane HC, et al. DAVID: a web server for functional enrichment analysis and functional annotation of gene lists (2021 update). *Nucleic Acids Res.* 2022;50:W216–W221.

ACKNOWLEDGEMENTS

This work was supported by Tenovus Cancer Care Wales (to RR and AT), Health and Care Research Wales (the Wales Cancer Research Centre) (to ED and AT), and the Fulbright Program (to PD, hosted by AT). SS, ED and AT were funded by the Myrovlytis Trust. We acknowledge our colleagues at Wales Gene Park for their insight and expertise in assisting with this research and for their technical and bioinformatic support. Wales Gene Park is an infrastructure support group funded by the Welsh Government by Health and Care Research Wales. Mass spectrometry and proteomics work was supported by the U.S. National Institutes of Health (NIH) Grant P20GM103449 from the INBRE program of the NIGMS. AP was funded by the Kidney Foundation of Canada (KFOC100021), the Myrovlytis Trust, the Terry Fox Foundation team grant on Oncometabolism (116128), and was a recipient of the Canada

Research Chair in Molecular Oncology. ACH is funded by the Myrovlytis Trust (grant number MT21_6).

AUTHOR CONTRIBUTIONS

RR, EAD, JDC, PFD, TC, ZJ, SS, OH and ART carried out the experiments, data interpretation and figure assembly. Bioinformatic analysis was performed by RR, EAD, PFD, IP, and PG. Bioinformatics data were assembled by RR, IP and ART. For mass spectrometry, samples were prepared by EAD and processed by PFD and BAB. *C. elegans* experiments were performed by ZJ and AP. The project was coordinated by ART with input from BJC, ACH and AP. The manuscript was written by EAD and ART and was proofread/edited by all.

COMPETING INTERESTS

The authors declare no competing financial interests. While this study is funded in part by Health and Care Research Wales, the views expressed are those of the authors and not necessarily those of Health and Care Research Wales or the Welsh Government.

ADDITIONAL INFORMATION

Supplementary information The online version contains supplementary material available at <https://doi.org/10.1038/s41388-025-03325-z>.

Correspondence and requests for materials should be addressed to Andrew R. Tee.

Reprints and permission information is available at <http://www.nature.com/reprints>

Publisher's note Springer Nature remains neutral with regard to jurisdictional claims in published maps and institutional affiliations.



Open Access This article is licensed under a Creative Commons Attribution 4.0 International License, which permits use, sharing, adaptation, distribution and reproduction in any medium or format, as long as you give appropriate credit to the original author(s) and the source, provide a link to the Creative Commons licence, and indicate if changes were made. The images or other third party material in this article are included in the article's Creative Commons licence, unless indicated otherwise in a credit line to the material. If material is not included in the article's Creative Commons licence and your intended use is not permitted by statutory regulation or exceeds the permitted use, you will need to obtain permission directly from the copyright holder. To view a copy of this licence, visit <http://creativecommons.org/licenses/by/4.0/>.

© The Author(s) 2025